Chinese Chemical Letters 31 (2020) 1030–1033

Contents lists available at ScienceDirect

Chinese Chemical Letters

journal homepage: www.elsevier.com/locate/cclet

Communication

Facile hydrothermal construction of Nb_2CT_x/Nb_2O_5 as a hybrid anode material for high-performance Li-ion batteries

Li Qin, Senyang Xu, Yang Liu, Shuhao Zhu, Linrui Hou*, Changzhou Yuan*

School of Material Science & Engineering, University of Jinan, Ji'nan 250022, China

ARTICLE INFO

Article history:
Received 9 February 2020
Received in revised form 29 February 2020
Accepted 2 March 2020
Available online 3 March 2020

Keywords:
Niobium-based MXene
Nb_2CT_x/Nb_2O_5
Hydrothermal construction
Hybrid anodes
Lithium ion batteries

ABSTRACT

Herein, a simple yet efficient hydrothermal strategy is developed to *in-situ* convert multi-layered niobium-based MXene (Nb_2CT_x) to hierarchical Nb_2CT_x/Nb_2O_5 composite. In the hybrid, the Nb_2O_5 nanorods are well dispersed in and/or on the Nb_2CT_x. Thanks to the synergetic contributions from the high capacity of Nb_2O_5 and superb electrical conductivity of the two-dimensional Nb_2CT_x itself, the resultant Nb_2CT_x/Nb_2O_5 hybrid exhibits excellent rate behaviors and stable long-term cycling behaviors, when evaluated as anodes for Li-ion batteries.

Over the past decades, Li-ion batteries (LIBs) have been widely used in daily life as the most mature energy storage devices, such as portable electronic devices, large power grids, and electric vehicles [1,2]. The graphite is the most conventional commercial anode material for LIBs, however, it always cause unstable solid electrolyte interphase (SEI) layer and lithium dendrites, due to its low lithiation voltage (~0.1 V *vs.* Li^+/Li). In addition, the rate capability and cycle stability of graphite are not satisfactory [3,4]. Therefore, it is necessary to develop an anode material with even higher lithiation voltage and rate behaviors. Typically, TiO_2 [5] and $Li_4Ti_5O_{12}$ [6] can be potential candidates due to their higher operating potential and excellent rate capability. But they are limited by lower theoretical capacities of ~170 mAh/g [5,6]. As an intercalation anode material, Nb_2O_5 has a large theoretical specific capacity of ~200 mAh/g, along with a small volume expansion rate of only ~3% compared to other alloy-type materials, which ensures the structural stability of Nb_2O_5-based electrodes during repeated charge-discharge cycles, and excellent electrochemical properties [7–9].

However, the Nb_2O_5 is limited seriously by its intrinsic modest conductivity. To date, most researches generally focus upon constructing carbon-based Nb_2O_5 materials to increase the electronic conductivity, such as Nb_2O_5@C [8], Nb_2O_5/C nanocomposites [10], Nb_2O_5/graphene [11–14]. In recent years, two-dimensional (2D) transition metal carbide (MXene) has emerged, which has high electrical conductivity, stable 2D structure. So, it would be expected as excellent conductive substrates [15–20].

At present, the most studied MXene is the Ti-based MXene. As previously reported, $Ti_3C_2T_x/TiO_2$ composites can be prepared directly from $Ti_3C_2T_x$ by hydration reaction [21]. And the hybrid $Ti_3C_2T_x/TiO_2$ shows good electrochemical Li-storage performance. Unfortunately, few reports about partial oxidation of the niobium-based MXene (denoted as Nb_2CT_x) towards efficient synthesis of Nb_2CT_x-based hybrids for electrochemical charge-storage applications can be retrieved so far.

Herein, the Nb_2O_5 nanorods (NRs) were first *in-situ* grew on the multi-layered Nb_2CT_x surfaces through a simple one-step mild hydrothermal avenue, where the Nb_2CT_x acted both as the niobium source and conducting medium. This strategy simultaneously stabilized the 2D structure of Nb_2CT_x, and rendered a hierarchical Nb_2CT_x/Nb_2O_5 hybrid. The Nb_2CT_x as a conductive matrix made up for the poor electrical conductivity of the Nb_2O_5, and the retained 2D structure was conducive to the rapid Li^+ transport. Encouragingly, the hybrid Nb_2CT_x/Nb_2O_5 exhibited excellent rate performance, stable reversible capacity, and long cycle life, highlighting its enormous potential in the practical application of LIBs.

The hybrid Nb_2CT_x/Nb_2O_5 was prepared as follows. Firstly, 2.0 g of Nb_2AlC powder (11 technology Co., Ltd.) was added in 20 mL of HF solution (50 wt%). After stirred at room temperature (RT) for 90 h, the suspension was centrifuged at 3500 rpm and washed with deionized (DI) water until the pH value of the solution went up to 6. And dried at 60 °C for 24 h in vacuum, the Nb_2CT_x power was obtained. Secondly, 0.5 g of the resulted Nb_2CT_x was added into

* Corresponding authors.
E-mail addresses: mse_houlr@ujn.edu.cn (L. Hou), mse_yuancz@ujn.edu.cn, ayuancz@163.com (C. Yuan).

https://doi.org/10.1016/j.cclet.2020.03.006

40 mL of DI water. After magnetic stirring for 20 min, the solution was poured into an autoclave (50 mL) and kept at 180 °C for 12 h. After washed with DI water and dried at 60 °C for 12 h under vacuum, the hybrid Nb_2CT_x/Nb_2O_5 was finally obtained.

Structures and morphologies of samples were investigated by X-ray powder diffraction (XRD, Rigaku Ultima IV), field-emission scanning electron microscopy (FESEM, JEOL-6300 F, 15 kV), transmission electron microscopy (TEM), scanning TEM (STEM), selected area electron diffraction (SAED) and high-resolution TEM (HRTEM) (JEOL JEM 2100 system) with an energy dispersive X-ray spectroscopy (EDS) system.

Electrochemical properties of samples were tested on 2032 coin-type cells. The working electrodes slurry were prepared by mixing as-prepared active materials (80 wt%) with carbon black (10 wt%) and polyvinylidene fluoride in *N*-methylpyrrolidone. After grinding and coating the mixture on the copper foil current collector, the pole pieces were dried in vacuum at 110 °C for 24 h. Metal lithium and a polypropylene film are used as the counter electrode and a separator, along with 1.0 mol/L $LiPF_6$ in a mixture of ethylene carbonate/diethylene carbonate (1:1, v/v) as the electrolyte. All cells were assembled in an Ar-filled glove box (MBRAUN) with the concentrations of O_2 and H_2O < 0.1 ppm. Galvanostatic charge/discharge tests were conducted with the voltage range of 1.0–3.0 V (*vs.* Li/Li^+) by a LAND test system (Land CT2001A). Cyclic voltammetry (CV) measurements were conducted on an IVIUM electrochemical workstation (The Netherlands).

Here, we characterize the morphologies of hybrid Nb_2CT_x/Nb_2O_5 by FESEM and (HR)TEM techniques. Obviously, accordion-like Nb_2CT_x (Fig. 1a) is successfully prepared with the HF acid etching. And the multi-layered MXene Nb_2CT_x still well maintains the 2D structure after hydrothermal reaction (Fig. 1b). One especially notes that there are some cylindrical shape nanorods (NRs) appearing on the surface of the nanosheets (NSs), and some even located between the NSs (Figs. 1b and c). Furthermore, the original smooth NSs become even rougher. Further TEM observation (Fig. 1b) evidences, besides the cylindrical NRs of larger size, the existence of smaller NRs *in-situ* grown on these NSs, which renders the rough the surface of the Nb_2CT_x NSs. For better revealing such phenomenon, hydrothermal reaction was further extended up to 24 h. These NRs has grown with even larger size appearing on the surface of NSs (Fig. S1 in Supporting information). Further HRTEM examination (Fig. 1d), corresponding to the blue circle region in panel (d), shows well-defined lattice fringes with a

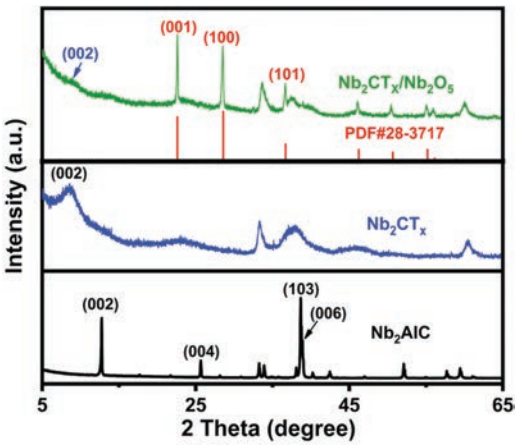

Fig. 2. Wide-angle XRD patterns of the Nb_2AlC, Nb_2CT_x and Nb_2CT_x/Nb_2O_5 as indicated.

spacing of ~0.393 nm (Fig. 1e), which can be well indexed to the (001) crystal plane of Nb_2O_5. According to the principle of minimum energy (Wulff theory) [22], the [001] crystal orientation of Nb_2O_5 is the preferred growth orientation, and the formed Nb_2O_5 crystals will preferentially grow into rod-like architecture along the direction. As is well known, some single-layered Nb_2CT_x are always generated during HF etching.

During the subsequent hydrothermal oxidation of Nb_2CT_x to Nb_2O_5, the single-layered MXene Nb_2CT_x scattered outside lacks the effects of −OH, −O or −F plasma and the constraints between layers, it is therefore much easier to grow into the NRs shape, and the size of the NRs is larger than those *in-situ* located on the surface of the NSs with a interlayer distance of 1.059 nm (Fig. 1f). The high-magnification (HR)TEM (Figs. 1g and h) further confirms the Nb_2O_5 NRs with discernable (101) crystal plane grown on the Nb_2CT_x NSs. The SAED pattern (the inset in panel g) also visualize the quasi-single crystal nature of these Nb_2O_5 NRs. STEM and corresponding EDS mapping images (Fig. 1i) manifest the uniform elemental distribution throughout the hybrid. Similarly, the Nb, O, and C are also evenly distributed throughout the cylindrical NRs (Fig. S2 in Supporting information).

The crystalline structure of the Nb_2AlC, Nb_2CT_x and Nb_2CT_x/Nb_2O_5 are characterized by the XRD technique. From the XRD pattern (Fig. 2), it can be seen that the characteristic peak of Nb_2AlC

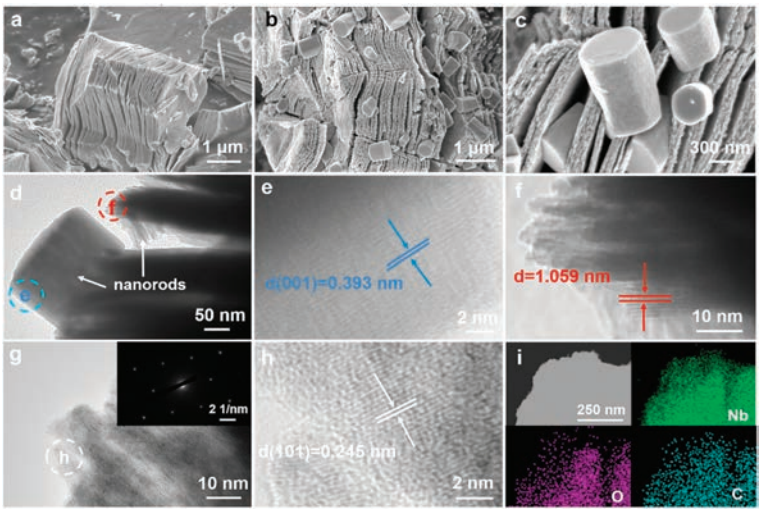

Fig. 1. FESEM images of (a) Nb_2CT_x and (b, c) Nb_2CT_x/Nb_2O_5. (d–h) TEM/(HR)TEM images, SAED pattern (the inset in panel g), (i) STEM and corresponding element (Nb, O and C) mapping images of Nb_2CT_x/Nb_2O_5.

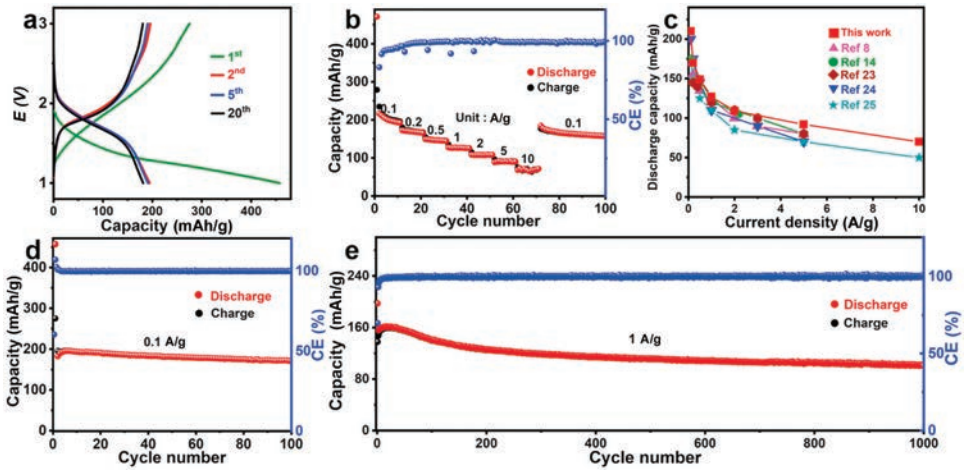

Fig. 3. Electrochemical performance of Nb_2CT_x/Nb_2O_5: (a) Galvanostatic charge-discharge plots at 0.1 A/g. (b) Rate behaviors. (c) Rate capability at various current rates from 0.1 A/g to 10 A/g. (d) Cycle performance at 0.1 A/g. (e) Long-term cycling performance at 1.0 A/g.

at 38.9° disappears in the Nb_2CT_x, and the shift and broadening of the (002) peak at 13.68° with HF acid etched, verifying the successful fabrication of multi-layered Nb_2CT_x, which is consistent with previous report [16]. As examined from the XRD diffraction reflections, it is easy to conclude that the co-existence of Nb_2CT_x and Nb_2O_5 in the product of Nb_2CT_x/Nb_2O_5, revealing the partial oxidation of the Nb_2CT_x into Nb_2O_5. Additionally, the (002) signal of Nb_2CT_x in the hybrid weakens somewhat, which results from the existence of the numerous Nb_2O_5 NRs on their surfaces. The main strong peaks centering at $2\theta = 22.3°$, 28.5° and 36.3° are well indexed to (001), (100) and (101) crystal planes of the *pseudo*-hexagonal Nb_2O_5 (JCPDS No. 28-3717) in the hybrid.

Thanks to the unique hybrid structures, the Nb_2CT_x/Nb_2O_5 electrode will be endowed with both the merits of the Nb_2CT_x and Nb_2O_5, and exhibits remarkable lithium-storage properties. Typical CV profiles (0.1 mV/s) recorded in the voltage of 1.0–3.0 V (*vs.* Li/Li^+) evidence a pair of cathodic/anodic peak centered at ~1.6 and 1.8 V, which are closely associated with the oxidation/reduction between Nb^{4+}/Nb^{5+} [2]. Fig. 3a demonstrates the selected voltage-capacity plots of the hybrid Nb_2CT_x/Nb_2O_5 anode. Apparently, the initial discharge and charge capacities are estimated as ~456 and ~275 mAh/g respectively, corresponding to the 1st Coulombic efficiency (CE) value of ~60.3%. The irreversible capacity loss should be ascribed to the electrolyte decomposition and formation of the SEI layer [21]. More strikingly, the anode still can retain reversible discharge/charge capacities as large as ~193.2/~193.3 mAh/g in 20th cycle, along with a high CE value of ~99.9%. Besides this, the Nb_2CT_x/Nb_2O_5 hybrid also shows very good capacity retention and stability in the process of increasing current densities, as profiled in Fig. 3b. At a current density of 0.1 A/g, the average discharge capacity of the hybrid anode is estimated as approximately 200 mA/g. When it further rises to 0.2, 0.5, 0.1, 2.0, 5.0 and 10 A/g, the hybrid Nb_2CT_x/Nb_2O_5 still can be stabilized as ~180, ~150, ~125, ~100, ~85 and ~65 mAh/g, respectively, that is, the capacity retention of 32.5% with the 50-time increase in current density. More appealingly, with the current density returning back to 0.1 A/g, the specific capacity still can be recovered at about 190 mAh/g, highlighting the exceptional electrochemical reversibility and rate performance of the Nb_2CT_x/Nb_2O_5 electrode. More competitively, the high-rate behaviors of our Nb_2CT_x/Nb_2O_5 are better than other Nb_2O_5-based anodes, for instance, Nb_2O_5 nanofibers (~110 mAh/g at 1 A/g) [23], Nb_2O_5 nanowires/graphene (~80 mAh/g at 5 A/g) [24], T-Nb_2O_5/GCN (~50 mAh/g at 10 A/g) [25], pure Nb_2CT_x (~50 mAh/g at 1.0 A/g) [26,27], as summarized in Fig. 3c. Fig. 3d demonstrates the cycle performance of the hybrid at a current density of 100 mA/g. Appealingly, the Nb_2CT_x/Nb_2O_5 electrode shows a small attenuation, and can maintain a high discharge capacity of ~190 mAh/g, much better than that of the commercial Nb_2O_5 (~99.8 mAh/g, Fig. S4 in Supporting information). More encouragingly, under a large current density of 1.0 A/g (Fig. 3e), the hybrid anode still can deliver a discharge as large as ~102 mAh/g over 1000 consecutive charge-discharge cycles, corresponding to a small capacity decay of 0.058 mAh/g per cycle, which indicates that the Nb_2CT_x/Nb_2O_5 anode possess excellent cycle stability even under high current density.

In summary, a simple yet efficient hydrothermal strategy is developed to *in-situ* convert multi-layered niobium-based MXene (Nb_2CT_x) to hierarchical Nb_2CT_x/Nb_2O_5 composite. Benefitting from the synergistic contribution of 2D conductive Nb_2CT_x and high-capacity Nb_2O_5, the hybrid Nb_2CT_x/Nb_2O_5 was endowed with convenient ionic and electronic diffusion/transport, and exhibited excellent rate performance (~65 mAh/g at 10 A/g) and long cycle performance (~102 mAh/g after 1000 cycles at 1 A/g). More significantly, our research here provides a simple and feasible strategy to construct high-performance Nb_2CT_x-based anodes for advanced LIBs.

Declaration of competing interest

The authors declare that they have no known competing financial interests or personal relationships that could have appeared to influence the work reported in this paper.

Acknowledgments

The authors acknowledge the financial support from the National Natural Science Foundation of China (Nos. 51772127 and 51772131), Taishan Scholars (No. ts201712050), Major Program of Shandong Province Natural Science Foundation (No. ZR2018ZB0317), Natural Science Doctoral Foundation of Shandong Province (No. ZR2019BEM038), Natural Science Doctoral Foundation of the University of Jinan (No. XBS1830) and Collaborative Innovation Center of Technology and Equipment for Biological Diagnosis and Therapy in Universities of Shandong.

Appendix A. Supplementary data

Supplementary material related to this article can be found, in the online version, at doi:https://doi.org/10.1016/j.cclet.2020.03.006.

References

[1] J.B. Goodenough, K.S. Park, J. Am. Chem. Soc. 135 (2013) 1167–1176.
[2] Q.L. Deng, Y.P. Fu, C.B. Zhu, Small 15 (2019) 1804884.
[3] L.J. Yang, X. Cheng, Y. Gao, et al., RSC Adv. 4 (2014) 26335–26341.
[4] V.A. Agubra, J.W. Fergus, J. Power Sources 268 (2014) 153–162.
[5] H. Ren, R.B. Yu, J.Y. Wang, et al., Nano Lett. 14 (2014) 6679–6684.
[6] T. Yuan, Z.P. Tan, C.R. Ma, et al., Adv. Energy Mater. 7 (2017) 1601625.
[7] D.C. Chen, J.H. Wang, T.F. Chou, et al., J. Am. Chem. Soc. 139 (2017) 7071–7081.
[8] E. Lim, C. Jo, H. Kim, et al., ACS Nano 9 (2015) 7497–7505.
[9] K.J. Griffith, A.C. Forse, J.M. Griffin, C.P. Grey, J. Am. Chem. Soc. 138 (2016) 8888–8899.
[10] G.Y. Zeng, H. Wang, J. Guo, et al., Chin. Chem. Lett. 28 (2017) 755–758.
[11] L.P. Kong, X.D. Cao, J.T. Wang, et al., J. Power Sources 309 (2016) 42–49.
[12] H.T. Sun, L. Mei, J.F. Liang, et al., Science 356 (2017) 599–604.
[13] L.P. Wang, L.H. Yu, R. Satish, et al., RSC Adv. 4 (2014) 37389–37394.
[14] P. Arunkumar, A.G. Ashish, B. Babu, et al., RSC Adv. 5 (2015) 59997–60004.
[15] B. Anasori, M.R. Lukatskaya, Y. Gogotsi, Nat. Rev. Mater. 2 (2017) 1–17.
[16] M. Naguib, J. Halim, J. Lu, et al., J. Am. Chem. Soc. 135 (2013) 15966–15969.
[17] C.F. Zhang, M. Beidaghi, M. Naguib, et al., Chem. Mater. 28 (2016) 3937–3943.
[18] Y. Xiao, J.Y. Hwang, Y.K. Sun, J. Mater, Chem. A 4 (2016) 10379–10393.
[19] J.J. Yin, F.K. Zhan, T.F. Jiao, et al., Chin. Chem. Lett. 31 (2020) 992–995, doi: http://dx.doi.org/10.1016/j.cclet.2019.08.047.
[20] Q. Wang, S.Y. Chu, S.H. Guo, Chin. Chem. Lett. (2019), doi:http://dx.doi.org/10.1016/j.cclet.2019.12.008.
[21] C. Yang, Y. Liu, X. Sun, et al., Electrochim. Acta 271 (2018) 165–172.
[22] L. Fei, D.F. Xue, Phys. Scripta (2010) 014074.
[23] J.Y. Cheong, J.W. Jung, D.Y. Youn, et al., J. Power Sources 360 (2017) 434–442.
[24] H. Song, J.J. Fu, K. Ding, et al., J. Power Sources 328 (2016) 599–606.
[25] D. Li, J. Shi, H.L. Liu, et al., Sustain. Energy Fuel 3 (2019) 1055–1065.
[26] R. Butt, A.H. Siddique, S.W. Bokhari, et al., Int. J. Energy Res. 43 (2019) 4995–5003.
[27] R. Liu, W.K. Cao, D.M. Han, et al., J. Alloys Compd. 793 (2019) 505–511.